Ultrasonics Sonochemistry 93 (2023) 106290

Contents lists available at ScienceDirect

Ultrasonics Sonochemistry

journal homepage: www.elsevier.com/locate/ultson

Experiment investigation on effects of elastic modulus on cavitation erosion of silicone rubber

Yangjun Wang [a,b], Ziyuan Li [a,b], Limei Tian [a,b,*], Zhen Shang [a,c]

[a] Key Laboratory of Bionic Engineering, Ministry of Education, Jilin University, Changchun 130022, China
[b] Weihai Institution for Bionic, Jilin University, Weihai 264400, China
[c] School of Mechanical and Aerospace Engineering, Jilin University, Changchun 130022, China

ARTICLE INFO

Keywords:
Cavitation erosion
Elastic modulus
Coating

ABSTRACT

Research into cavitation phenomena in various fields shows that the elastic modulus of a boundary has a potential impact on cavitation erosion. To obtain the direct relationship between the elastic modulus of the boundary and cavitiation erosion, single-layer samples with different chemical composition and moduli, and double-layer samples with different elastic moduli and the same surface layer material, were prepared with silicone rubber. The results of cavitation experiments on single-layer samples, show that the coating chemical composition and mechanical properties together affect the cavitation morphology of the coating, and dominant factors vary with erosion stage. Through the cavitation test of double-layer samples, it was found that there is a positive correlation between the elastic modulus of the coating and the degree of cavitation. This study helps us to understand the relationship between coating elastic modulus and cavitation more directly, and provides theoretical and technical guidance for the application of anti-cavitation for elastic coating in engineering.

1. Introduction

Cavitation corrosion seriously damages the performance of fluid machinery such as water pumps, propellers and so on, which will reduce their service life [1,2]. Numerous studies have been conducted on improving the cavitation resistance of materials by metal strengthening [3–5] and spraying [6,7], where organic polymer coatings [8–10] are considered to be one of the effective methods to protect flowing parts from cavitation. It is generally believed that there are two factors why organic polymer coatings can resist cavitation erosion: One is that the chemical properties of polymer materials are not easily corroded, and they can form a barrier between the fluid and protected parts. The other factor is that the elastic wall of a polymer coating interacts with bubbles.

Many scholars have made important progress in the interaction between cavitation bubbles and elastic surfaces. In these researchs, the coating is usually studied as an elastic surfaces, bubbles are mainly produced from electric spark discharge and laser induction. An electric spark discharge device is simple and widely used, Blake et al. [11,12] studied the interaction between coatings on rigid boundaries, free boundaries and flexible boundaries and bubbles generated by electric sparks and showed that the changes in cavitation bubbles near boundaries can be described by inertia and stiffness. C.K. Turangan [13] studied the interaction between cavitation bubbles and thin elastic membranes. The coupling between bubble shrinkage and flexible surface disturbances promotes bubble collapse and leads to the formation of mushroom-shaped bubbles, bubble squeezing and splitting. Aghdam [14] experimentally studied the interaction between two bubbles of similar size and the elastic film underneath. Goh [15] studied the interaction between bubbles and elastic spheres generated by sparks. Elasticity, dimensionless distance and the size ratio for bubbles and elastic spheres will affect the interaction mode. Laser-induced cavitation has also been extensively studied. Shaw [16] used schlieren photography and Mach-Zehnder interferometry to study the interaction between cavitation bubbles and flexible membranes and observed that the movement of a flexible membrane surface is inconsistent during bubble generation and rupture. Sankin [17] found that a bubble with the best shock wave arrival time and separation distance can produce the largest jet and penetrate into the membrane when it bursts. Brujan et al. [18–20] observed the interaction between the bubbles generated by a laser and the elastic boundary of a polyacrylamide gel with a modulus of 0.017–2.030 MPa and analyzed the formation of mushroom bubbles far away from the boundary. The formation of a jet, the formation of a radial jet that causes the bubble to split and the subsequent formation of two jets in opposite directions, the liquid jet entering the boundary, and

* Corresponding author at: Key Laboratory of Bionic Engineering, Ministry of Education, Jilin University, Changchun 130022, China.
E-mail address: lmtian@jlu.edu.cn (L. Tian).

https://doi.org/10.1016/j.ultsonch.2023.106290
Received 18 October 2022; Received in revised form 27 December 2022; Accepted 4 January 2023
Available online 5 January 2023

the deformation of the boundary material. They found that the jet penetration at the boundary and the deformation generated by tensile stress in the process of bubble collapse lead to boundary erosion. The work of Gong et al. [21] is of great significance: They studied the scale relationship of bubbles produced by different external sources based on an improved Rayleigh model and experimental observations. The results showed that when studying large-scale and complex physical problems, sparks or laser-generated bubbles can be used to replace underwater explosion bubbles.

In addition, the cavitation damage mechanism on the coating surface has also received much attention. Dular et al. [22] used a thin aluminum foil stuck to the surface of a Venturi tube to study its cavitation corrosion. Through the image results, it was found that the cavitation cloud collapset with a spherical-shape, horseshoe-shaped and "distorted" -shape is the main damage mechanism. In addition, the moment of separation of the cavitation cloud and stagnation will also lead to cavitation corrosion. Hoon et al. [23] used coarse-grained molecular dynamics simulations to study the cavitation damage mechanism of polystyrene (PS) films. The research results shown that the damage is caused by collapsing nanobubbles located near the film and interaction with the shock wave. The polymer molecules located near the jet extend conformationally in the direction perpendicular to the jet's motion, while the chain molecules in the rest of the film are compressed. Xiangnian Qiao [24] noted that the cavitation resistance of the coating is related to the water resistance, hardness, adhesion strength and dynamic mechanical properties of a coating, and the cavitation resistance of a siloxane-modified polyurethane coating is better than that of a high-strength epoxy resin. Furthermore, several studies have shown that metal substrates and coatings interact with each other under impact. The higher hardness stainless steel substrate and the TiN coating have good adhesion properties, and the coating delamination is not easy to occur under the impact of cavitation, and has better anti-cavitation performance [25]. The entire depth of strain hardening caused by cavitation shock was deeper for higher hardness S235JR-AR steel (4 mm) than for lower hardness S235JR-TT steel (2.5 mm) [26]. The substrate behavior under impact load has a critical influence on cohesive failure, cohesive-adhesive failure [27], cracking and delamination [28].

Most of the above studies paid attention to the interaction process between coating elasticity and cavitation bubbles, but the relationship between the elastic modulus of coating and cavitation erosion was ignored. This is the valuable parts of elastic coatings application in engineering. To solve this practical problem and analyze the effect of elastic modulus of boundary materials on cavitation erosion, five kinds of silicone rubber samples with different elastic moduli were designed and tested for their cavitation resistance by an ultrasonic cavitation instrument. However, the chemical composition of silicone rubber with different moduli are also different, which cannot fully reflect the impact of coating mechanical properties on the anti-cavitation performance. For this reason, five samples of double-layer structures with different elasticity were prepared, where the surface layer in direct contact with water was composed of exactly the same material, while the bottom layer consisted of materials with different elastic moduli. In this way, differences in the chemical composition of the surface materials can be avoid to affect the experimental conclusions.

2. Experimental method

2.1. Materials and method

2.1.1. Materials

The silicone rubber with five different hardness (shore A hardness/molecular weight: 0/32000, 5/39000, 10/44000, 20/48000 and 30/53000) which can be prepared with different elstic moduli as basic matrix, was purchased from China Bluestar Chengrand Co., ltd, China. The curing agent (tetrapropoxysilane, a silicone rubber hardener) is purchased from Shanghai Macklin Biochemical Co., ltd, China.

2.1.2. Experimental materials preparation

In this paper, single-layer and double-layer silicone rubber samples with different elastic moduli and structure were prepared, where the single-layer samples were made of five different hardnesses of silicone rubbers with the following material preparation process: Firstly, 1.5 g of tetrapropoxysilane was added to 100 g of each of the five silicone rubbers with different hardness and stirred at 1500 rpm for 10 min. Secondly, the mixed silicone rubbers with different elastic moduli were placed in a vacuum chamber at 133 Pa for 30 min until the air bubbles completely escaped. Finally, the vacuumed silicone rubbers of each of the five different elastic moduli were poured into molds of 35 × 35 mm^2 (length × width) and 1 mm thickness and placed in a 60 °C environment to cure for 24 h. After waiting for curing then all experimental samples were continued to be cured at room temperature for one week to obtain five single-layer samples (S1, S2, S3, S4, and S5) with different elastic moduli, and the specific preparation process is shown in Fig. 1 (a, b, c, d).

For the double-layer samples, the bottom layer consisted of materials with different moduli and the thickness of 3 mm, the surface layer was the same material and only 1 mm thick. The bottom layer of the double-layer sample is three times the thickness of the surface layer in order to make the modulus of the double-layer sample closer to that of the bottom layer. The preparation process of the double-layer samples was the same as that of the single-layer samples, but the moulding process was different. The specific difference was that the silicone rubber with different elastic moduli (S1, S2, S3, S4, S5) was poured into a 35 × 35 mm^2 (length × width) mold with a thickness of 3 mm of the poured material. It was placed in a 60 °C environment to cure for 2 h. Subsequently, the evacuated silicone rubbers with the same elastic modulus of S2 were poured into the previously semi-solidified state of silicone rubbers with different elastic moduli, whose thickness were kept at 1 mm, and cured at an environment of 60 °C for 24 h. Double-layer samples with different elastic moduli (D1, D2, D3, D4, and D5) were obtained. Waiting for curing then all experimental samples were continued to be cured at room temperature for one week, the specific preparation process is shown in Fig. 1 (a, b, c, e). The pictures of cured single-layer and double-layer samples are shown in Fig. 1 (f).

Table 1 shows the different compositions of the double-layer samples and the densities of the single-layer samples (S1-S5) are shown in the Table 2.

2.2. Cavitation erosion resistance test

An ultrasonic cavitation tester machine (XOQS-2500, Nanjing Atpio Instrument Manufacturing Co., ltd, China) was equipped according to the ASTM G32-16 standard in water with a control system, as shown in Fig. 2. This system uses high-power ultrasonic waves to act on a sample to simulate the cavitation phenomenon for a contact surface between a sample and liquid, analyzes the cavitation resistance of the material and enables study of the inherent anti-cavitation performance of a given material and its process in detail. Here, distilled water was used as the cavitation medium, and the test temperature for water was maintained at 25 ± 0.2 °C by a temperature control system. The ultrasonic generator continued to work at a frequency of 20 kHz and an amplitude of 50 ± 2.5 μm, and the ultrasonic power was 2500 W. The horn was fabricated from titanium alloy with a diameter of 15.9 mm, and the test sample was firmly bonded onto a SUS 304 bracket by 3 M PR40 glue at a distance of 1 mm facing the cavitation horn tip surface. Clearance of 1 mm is widely used for cavitation testing of metals [29] and non-metals [30], so this representative clearance was selected in this study.Tests were carried out for the same type of samples with different durations, and the sample was cleaned and dried until the weight no longer changes; an analytical balance was used to measure the weight of each sample before and after the test, and then a cavitation curve was drawn.

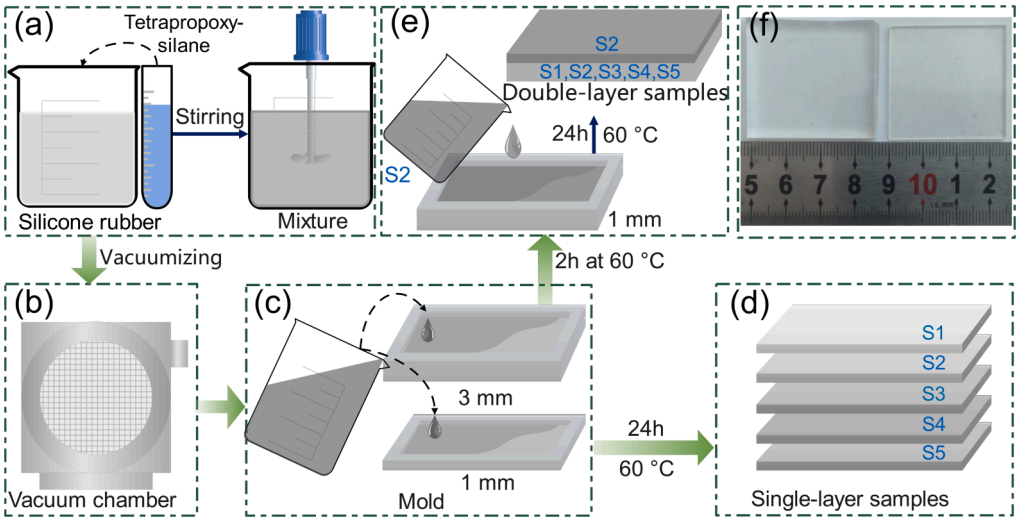

Fig. 1. (a-e) Preparation of the materials; (f) samples pictures.

Table 1
The structure of the double-layer samples.

Sample	D1	D2	D3	D4	D5
Surface layer (1 mm)	S2				
Bottom layer (3 mm)	S1	S2	S3	S4	S5

Table 2
Densities of the S1-S5.

Sample	S1	S2	S3	S4	S5
Density ($g \cdot cm^{-3}$)	1.14	1.15	1.15	1.16	1.15

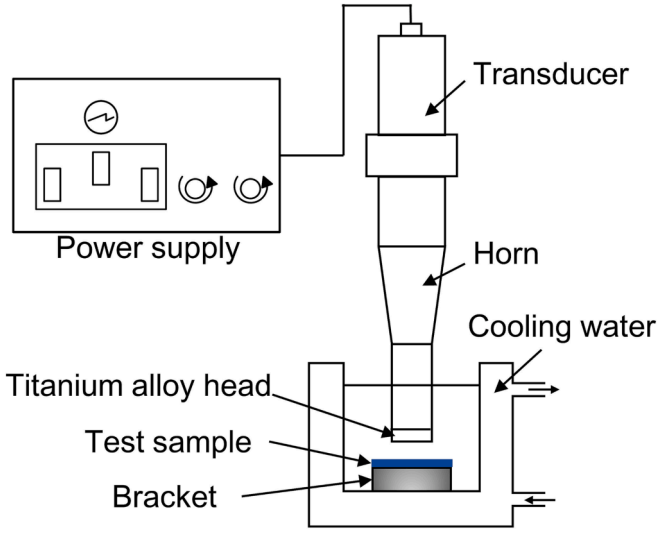

Fig. 2. Ultrasonic cavitation test device.

2.3. Analysis and characterization

Scanning electron microscope (VEGA3 TESCAN, Czechia) and white light interference microscopy (MFT-5000, Retc, USA) were used to analyze the erosion appearance and erosion degree of the sample. The depth data of all points were obtained by analyzing the 3D images with the data processing software Gwyddion and using origin 9.0 to analyze all depth data to obtain the depth distribution. XRD measurements were performed at ambient temperature using an X-ray single crystal diffractometer (R-AXIS RAPID II, Rigaku, Japan). The XRD patterns were obtained using CuKα radiation with a 2θ range of 5-60°. A Raman microscope (DXR 3xi, Thermo Scientific, USA) was used to analyze the material structure of the cavitation surface and the noncavitation area. The contact angle test utilized a drop shape analyzer (DSA25S, KRUSS). The elastic modulus tests were conducted using a rubber electronic tensile testing machine (UTM5305, Youhong Measurement and Control Technology Co., ltd, Shanghai, China), with a Transcell BSS-500 kg (accuracy of 0.01 N) force transducer and a compression speed of 5 mm/min. As shown in Fig. 3, the modulus of the double-layer samples were measured by the normal compression of the stack, the thicknesses of single-layer samples and double-layer samples used for modulus tests were 4 mm.

3. Results and discussion

3.1. Cavitation erosion for single-layer coatings with different elastic moduli

3.1.1. Cavitation erosion volume loss

As shown in Table 3, moduli of S1 to S5 increase form 0.16 MPa to 1.21 MPa. The modulus of silicone rubber is positively correlated with its molecular weight.

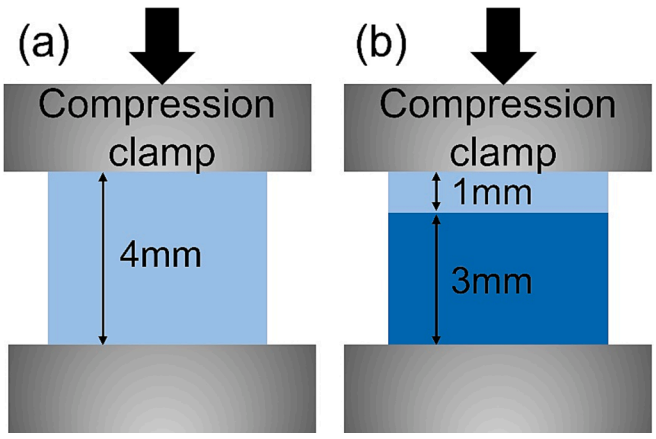

Fig. 3. Test method for elastic modulus of samples. (a) single-layer samples; (b) double-layer samples.

Table 3
Modulus and molecular weight of S1-S5.

Sample	S1	S2	S3	S4	S5
Modulus (MPa)	0.16	0.21	0.4	0.88	1.21
Molecular weight	32,000	39,000	44,000	48,000	53,000

The volume loss for a sample is an important and direct indicator to measure the anti-cavitation performance of a coating. Therefore, in this section, single-layer samples with five different elastic moduli were subjected to cavitation tests at 4 h, 8 h, 12 h and 24 h. The volume loss and the erosion rate for each sample at different stages were shown in Fig. 4. As shown in Fig. 4(a), for all samples, the volume loss of the samples showed an increasing trend with time. Among them, within 8 h of the initial stage, the volume loss of S1 is the largest, said, indicating that the anti-cavitation performance of S1 is poor at this stage. Moreover, within 12 h, the cavitation volume loss of S3 is smaller than that of the other four samples, indicating that S3 exhibits better anti-cavitation performance at this stage. When the cavitation test time of all samples reaches 24 h, the cavitation volume loss value of S2 is smaller than that of other samples, while the cavitation volume loss value of S5 increases rapidly, indicating that S5 has the worst anti-cavitation performance. As shown in Fig. 4(b), that the erosion rate reaches its first peak at 4 h, reaches the lowest point at 8 h or 12 h, and then increases slowly. The maximum erosion rates of S1 and S2 appeared at 4 h, S3 at 12 h, and S4 and S5 at 24 h.

3.1.2. Cavitation erosion morphology

Fig. 5 shows the surface morphology of different samples at different erosion stages. Through comparison, it can be observed that when the cavitation time is short, point defects exist on the surface of all samples. The pits for S1 are small in diameter but denser, the pits for S2-S4 are larger but sparsely distributed, and the pits for S5 are large and dense. With increasing cavitation time, point defects gradually increase and expand and continue to contact and fuse to form large pits, showing surface erosion and corrosion. The number and quality of pitting pits in the early stage of erosion are small, so the erosion volume loss is small. The expansion and fusion of pitting pits in the later stage of erosion is the main reason for the acceleration of erosion.

Fig. 6 (a- e) shows a 3D image of the eroded surface of S1-S5 at 24 h. With increasing cavitation time, not only do the density and diameter of the pits gradually increase, but their depths also increase significantly. In addition, in order to analyze the change of cavitation resistance at different time stages in Fig. 5, we take S5 as an example to test the contact angle of S5 surface at different stages. Fig. 6(f) shows that for the test time of 12 h, the contact angle of the sample surface increases slowly, when the test time exceeds 12 h, the contact angle of the sample surface increases rapidly. The surface of the sample is eroded by cavitation, which increases the surface roughness of the sample and increases the contact time with cavitation [31,32], which in turn accelerates the erosion process. In Fig. 7(a- d), the distribution data of cavitation pits on the surface of S1-S5 samples after 24 h of cavitation erosion test are given. S1 has a greater proportion of shallow pits, while S5 has a greater proportion of deep pits. As shown in Fig. 7(f), S2 has the smallest cavitation erosion depth, S5 has the maximum erosion depth.

3.1.3. Cavitation erosion affected by elastic modulus and chemical composition

XRD profile and raman spectra of single-layer samples shown in Fig. 8. The positions and widths of the main molecular groups of S1-S5 are the same, but the intensity of the groups decreases with increasing modulus. Meanwhile, their elastic moduli and hardness are positively correlated with molecular weight [33]. Obviously, for single-layer coatings, chananges of chemical composition lead to changes in mechanical properties.

The low elastic modulus coating can buffer the shock wave caused by cavitation bubbles, but its molecular chain is short, and the molecular chain is easily broken under the same impact strength, which explains why the volume loss of S1 in the early stage in Fig. 4 is very high. Although the high elastic modulus coating has a weak buffering effect on the cavitation shock wave, due to the high degree of cross-linking, the molecular chain is not easy to break under the impact, so in Fig. 4, although the volume loss of S5 is the largest in the later stage, it is relatively small in the early stage.

In the initial stage of erosion (0–8 h), the elastic modulus of sample S1 is lower, the volume loss of erosion is the largest, and there are small point-like defects on the surface. But the sample S5 with the highest elastic modulus, its volume loss is much smaller than that of S1. Fig. 9 shows the Raman spectra of the cavitation and nocavitation area of S2 at 24 h. The Raman spectral peak positions of the two regions are the same, but the Raman peak intensity observed in this region is significantly reduced after cavitation, which indicates that molecular chains on the surface of the cavitation region are broken and lost. This means that the elastic buffering effect of the coating has a weak effect on erosion, while the crosslinking of the coating plays an important role in the early erosion process. The larger the molecular weight of the coating, the less likely the molecular chain is to be destroyed by cavitation impact.The breakage of cavitation bubble damages the coating molecular chain is shown in Fig. 10(a).With the increase of test time (12–24 h), the volume loss of samples S4 and S5 with larger modulus increases rapidly, the advantage of high molecular weight coating weakens, but the effect of low elastic modulus begins to strengthen. As shown in Fig. 10(b),energy generated by cavitation rupture elastic deformation absorption of coating. The smaller the modulus of the coating, the greater the elastic deformation will be produced and the more the energy generated by cavitation rupture will be absorbed.

For the sample with the smallest modulus, a possible explanation for

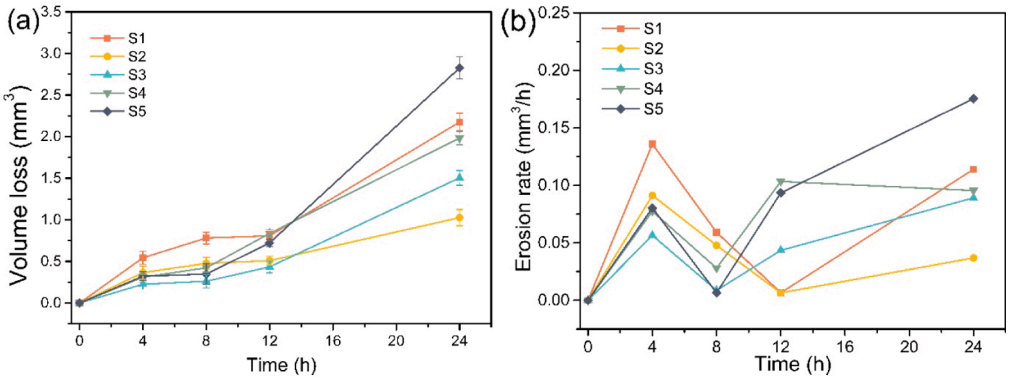

Fig. 4. (a) Volume loss for samples S1 to S5; (b) erosion rate for samples S1 to S5.

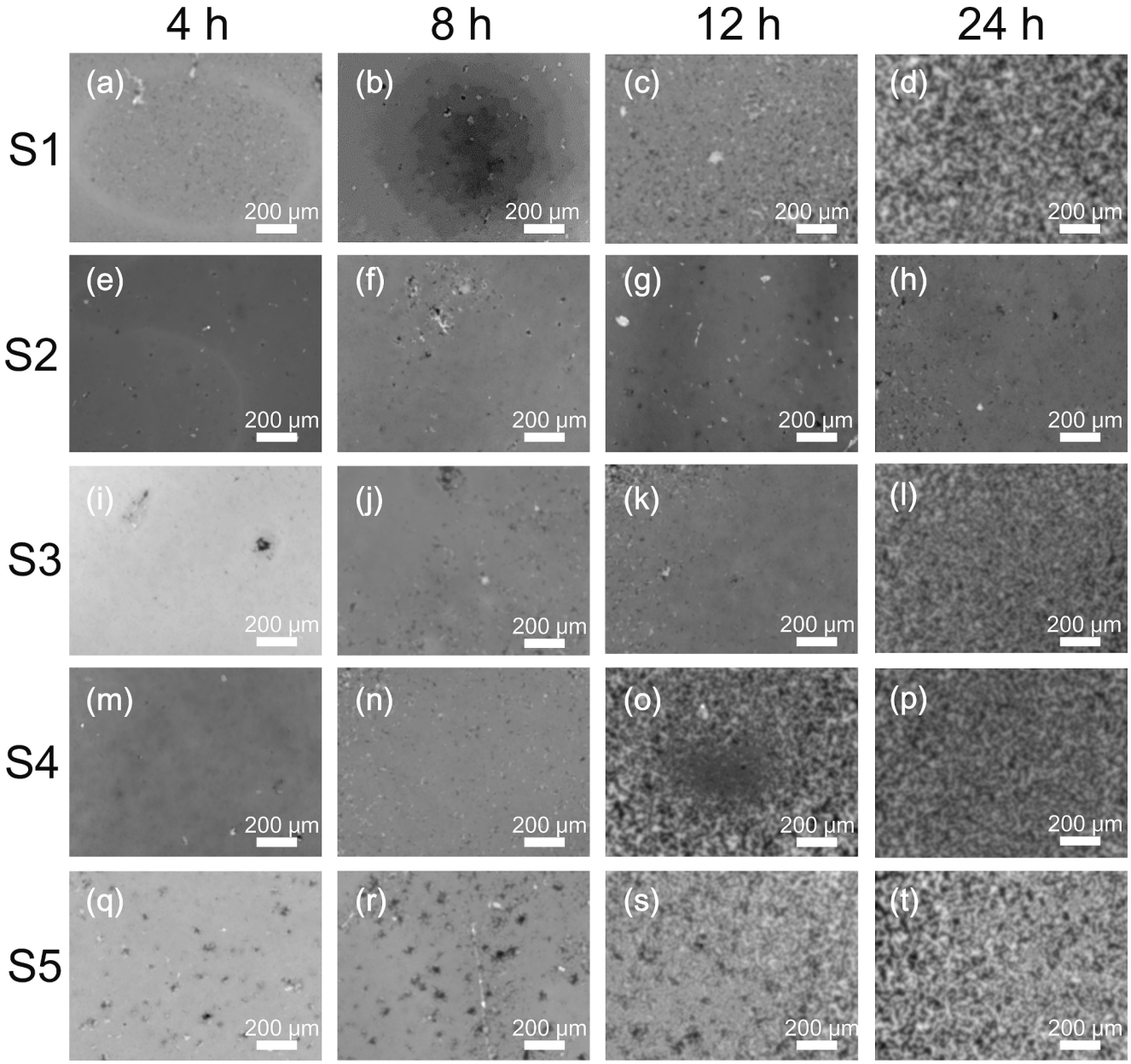

Fig. 5. Erosion micromorphology for S1-S5, (a- d) S1; (e- h) S2; (i- l) S3; (m- p) S4; (q- t) S5.

the volume loss of S1 is greater than that of S2 and S3 may be although the modulus of S1 is small, its elastic buffering effect is not enough to make up for the shortcoming of too small cross-linking degree, so its volume loss is always relatively high. These phenomena suggest that the chemical composition of the samples plays a dominant role in the cavitation characteristics in the early stage of erosion, while the role of mechanical properties is gradually enhanced in the later stage of erosion.

3.2. Cavitation erosion of the double-layer coatings

3.2.1. Cavitation erosion morphology

In Section 3.1, the cavitation resistance performance of the sample under the combined action of the material chemical composition and the mechanical properties is discussed. In this part, through analysis of the double-layer structure sample, the effect of the elastic modulus of the sample on the cavitation erosion performance is mainly discussed. Since the surface layer of the double-layer sample in contact with water and bubbles is the same material and has a thickness of only 1 mm, the bottom layer is composed of a material with a different modulus and a thickness of 3 mm. According to the relationship between coating deformation and thickness in literature [34], the impact generated by the rupture of the cavitation produces a deformation greater than 1 mm on the elastic surface with a modulus less than 2 MPa, therefore, the bottom layer of the double-layer sample in this study can also be deformed under the action of the cavitation shock wave, the double-layer sample can be regarded as an elastic body as a whole. In addition, it can be seen from the Fig. 6 that the maximum penetration depth of all samples after 24 h of cavitation test does not exceed 0.25 mm, therefore, cavitation erosion will not occur on the bottom layer. It can be considered that the double-layer materials have different moduli, but the surface chemical composition is consistent. Table 4 shows the moduli of D1-D5. The modulus of D1 slightly increases compared with S1. The modulus of D2 is the same as that of S2, and the moduli of D3, D4 and D5 is slightly smaller than that of S3, S4 and S5.

Fig. 11 shows the erosion morphologies of the double-layer sample

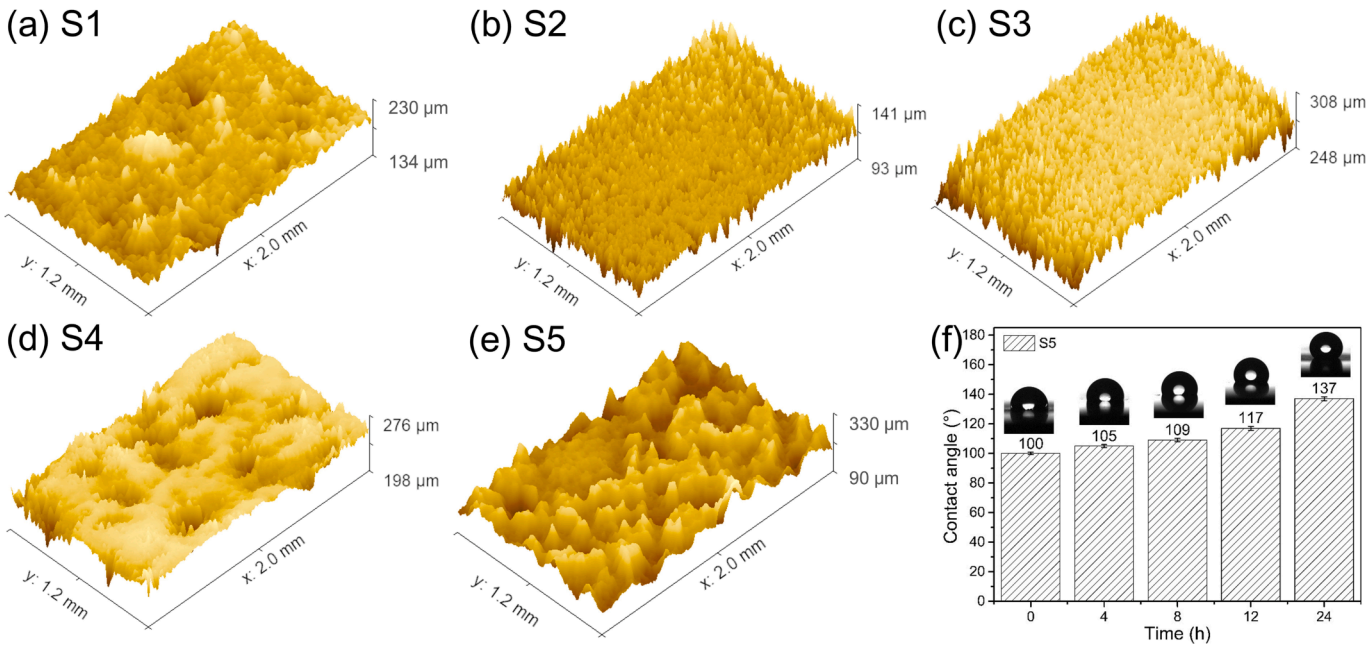

Fig. 6. (a-e) 3D image of a single-layer samples at 24 h; (f) Contact angle for the S5 cavitation area at different erosion times.

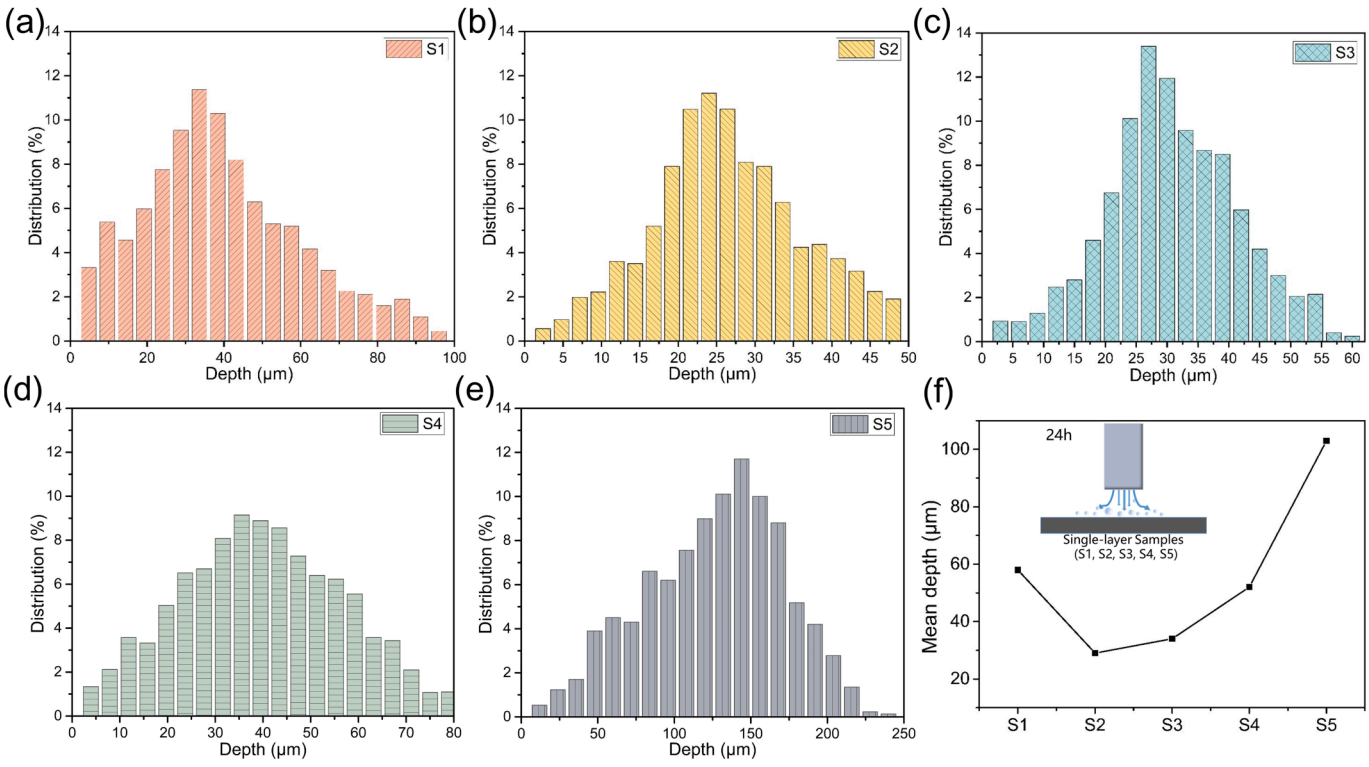

Fig. 7. (a- e) Depth distribution of S1-S5 coatings subjected to 24 h cavitation erosion; (f) mean depth of erosion of S1-S5 at 24 h.

after 12 h of cavitation. The erosion for D1 and D2 is the least obvious, with only sporadic pitting erosion observed. D3 and D4 show more obvious erosion, and the density of the pitting pits increases significantly. Due to the trend for mutual fusion, D5 erosion is the most serious, the pitting erosion pits in some areas are fused with each other, and there is basically no uneroded area. Fig. 12 shows the 3D images of the eroded surfaces of the five double-layer samples and the mean erosion depth for each of them. The surfaces for all eroded areas show different degrees of pitting characteristics. It can be clearly observed that the mean depth of erosion for D1 and D2 are shallower, and the mean depth of erosion for D5 is the deepest. This shows that as the degree of erosion increases, not only the number and area of erosion pits increase but also the depth of erosion pits also increases.

3.2.2. *The effect of elastic modulus alone on cavitation erosion*

Fig. 13(a) shows the erosion volume loss curve for the double-layer samples. Consistent with the erosion morphology characteristics, the volume loss increases with the increase of modulus for all test times, the

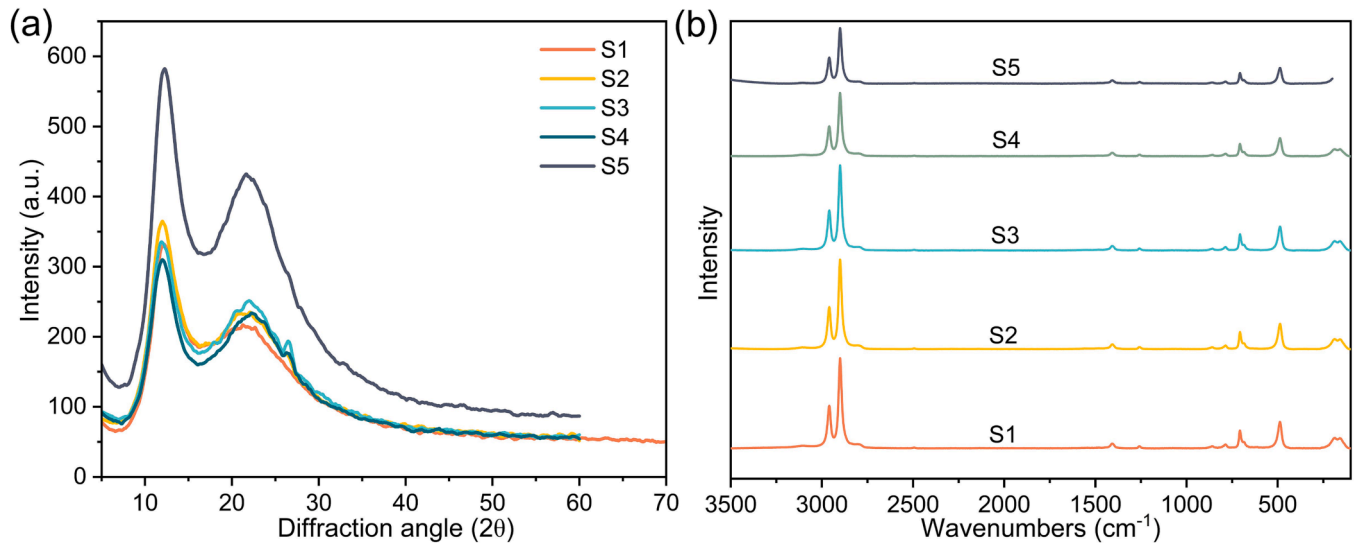

Fig. 8. (a) XRD profile and (b) raman spectra of single-layer samples.

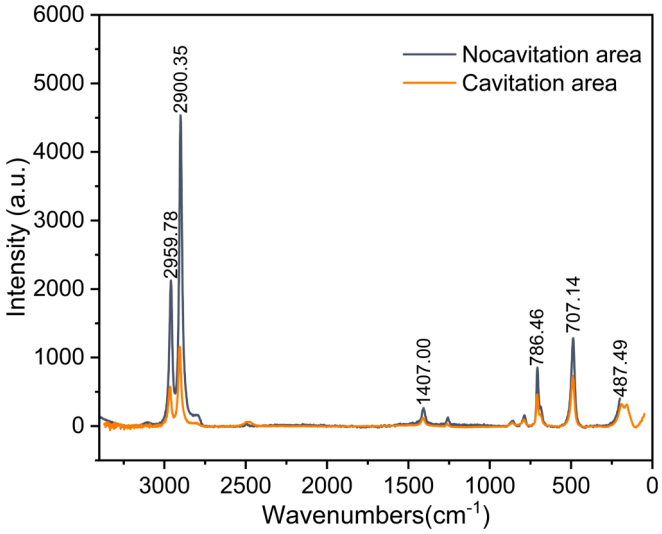

Fig. 9. Raman spectra for the cavitation area and noncavitation area of S2 at 24 h.

cavitation resistance is negatively correlated with the modulus. In addition, the chemical composition of D2 and S2 are identical only with different thicknesses, but there is little difference in volume loss between them. The volume loss of S2 is slightly higher than that of D2 but less than that of D3. As shown in Fig. 13(b), since the double-layer samples exclude the interference of coating chemical composition, the obtained law is different from the complex law between the modulus and volume loss revealed by the single-layer sample experiment.

From the perspective of energy, Govinaa Rao [35] proposed a dimensionless number C_D for cavitation, which represents the ratio of the energy absorbed by the coating surface to the energy released when the cavitation bubbles collapse

$$C_D = \frac{E\sum_0^n i}{np_0R_0} \tag{1}$$

where E (J·mm^{-3}) is the energy absorbed by the deformation of the coating per unit volume, i (mm), R_0 (mm) and n were average depth, maximum radius and number of erosion pits, P_0 (Pa)is pressure of the liquid around the bubble. According to this formula, only when C_D is equal to 1, all the energy released by the bursting of the cavitation bubbles is used to break the coating molecular chain. But in reality, C_D is less than 1 due to coating elasticity and other factors, part of the energy is temporarily stored in the form of elastic potential energy, and not all of it is used to erode the coating. So this really illustrates the potential role of elastic modulus in this cavitation erosion process.

Table 4
Modulus of D1-D5.

Sample	D1	D2	D3	D4	D5
Modulus (MPa)	0.17	0.21	0.37	0.76	1.09

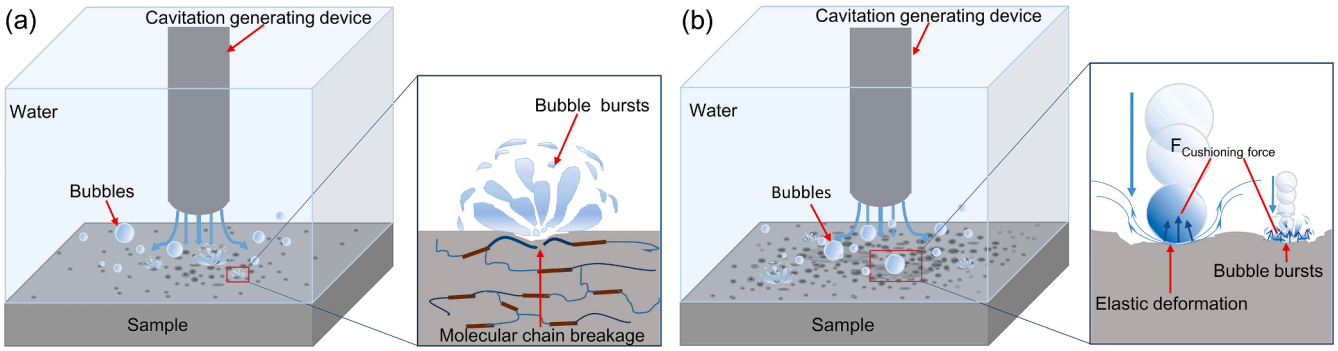

Fig. 10. (a) The breakage of cavitation bubble damages the coating molecular chain; (b) the elastic deformation of the coating absorbs the cavitation impact energy.

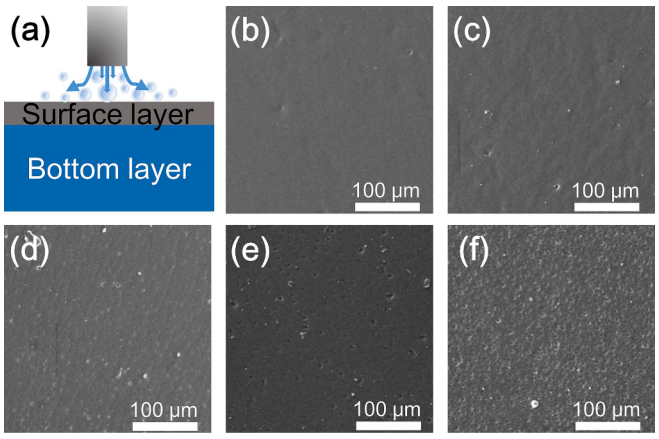

Fig. 11. Erosion micromorphologies (SEM) for a double-layer samples at 12 h, (a) Schematic diagram of the double-layer structure; (b- f) SEM of D1- D5.

The elastic coating can be elastically deformed during the shock wave and jet flow generated when a bubble bursts, dispersing the shock load generated when the bubble bursts. This dispersing effect can be summarized in two ways: One is the increase in the impact area, and the other is that the shock wave continues to propagate inside the coating after penetrating the surface of the sample, dispersing the surface shock into the volume space. On the premise that the deformation of a surface does not exceed the deformation limit of a material, the generation of cavitation is avoided. When the modulus gradually increases, the dispersion effect for surface deformation on the impact load is weakened, and cavitation erosion is more likely to occur. In addition, there exist situations that do not appear in this study, when the deformation of a coating exceeds the limit strain of a material, the coating will also be damaged. This situation is closely related to the position of the cavitation. In an actual hydraulic component, coating design should be emphatically considered.

4. Conclusions

The anti-cavitation performance of a coating is affected by many factors, and the mechanical properties of a coating are one of the important factors. The elastic modulus of a coating has an important

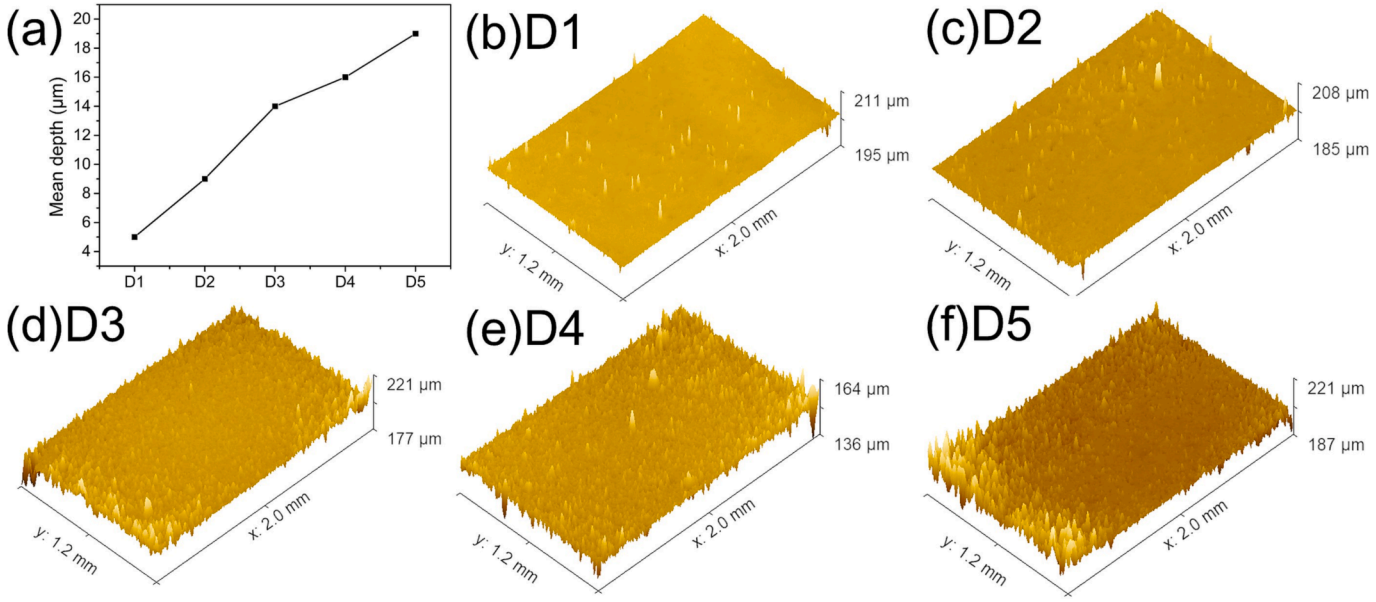

Fig. 12. (a) Mean erosion depths of the five double-layer samples (D1-D5) at 12 h; (b- f) 3D images of each of the five double-layer samples at 12 h.

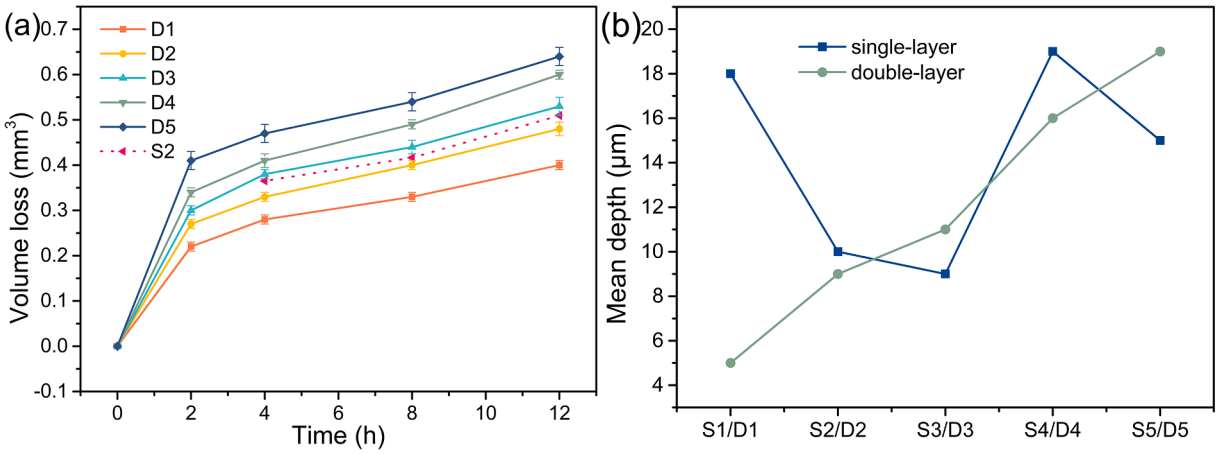

Fig. 13. (a) Volume loss for double-layer samples; (b) mean depth of erosion for 12 h cavitation test of single-layer and double-layer samples.

influence on the dynamic interaction between a cavitation bubble and coating, which in turn determines the cavitation resistance of a coating to a certain extent. This study establishes a more direct relationship between the elastic modulus and cavitation resistance performance through cavitation tests for coatings with different elastic moduli and structure. The results show that when the elastic modulus is less than 1.09 MPa, and does not consider the influence of coating chemical composition, cavitation resistance decreases with increasing modulus. This study provides a reference for the design of anti-cavitation erosion coatings for flow-through components.

CRediT authorship contribution statement

Yangjun Wang: Investigation, Writing – original draft. **Ziyuan Li:** Methodology, Writing – original draft. **Limei Tian:** Conceptualization, Writing – review & editing, Funding acquisition. **Zhen Shang:** Validation, Writing – review & editing.

Declaration of Competing Interest

The authors declare that they have no known competing financial interests or personal relationships that could have appeared to influence the work reported in this paper.

Acknowledgements

The authors are grateful for grants received from the Foundation for Innovative Research Groups of the National Natural Science Foundation of China (No. 52021003), the National Natural Science Foundation of China General Program (Grant No. 51875240), the Program for Jilin University Science and Technology Innovative Research Team (Grant No. 2020TD-03), the Young and Middle-aged Technology Innovation Leading Talents and Team Projects of Science and Technology Development Plan of Jilin Province(Grant No. 20200301013RQ).

References

[1] A. Adamkowski, A. Henke, M. Lewandowski, Resonance of torsional vibrations of centrifugal pump shafts due to cavitation erosion of pump impellers, Eng. Fail. Anal. 70 (2016) 56–72, https://doi.org/10.1016/j.engfailanal.2016.07.011.
[2] L. van Wijngaarden, Mechanics of collapsing cavitation bubbles, Ultrason. Sonochem. 29 (2016) 524–527, https://doi.org/10.1016/j.ultsonch.2015.04.006.
[3] A. Rajput, J. Ramkumar, K. Mondal, Effect of addition of strong oxidizer and temperature on the cavitation erosion resistance of different microstructures made from a high carbon steel, Wear 494–495 (2022), 204245, https://doi.org/10.1016/j.wear.2022.204245.
[4] I. Mitelea, I. Bordeaşu, E. Riemschneider, I.D. Uţu, C.M. Crăciunescu, Cavitation erosion improvement following TIG surface-remelting of gray cast iron, Wear 496–497 (2022), 204282, https://doi.org/10.1016/j.wear.2022.204282.
[5] D.B. Oliveira, A.R. Franco, A.C. Bozzi, Influence of low temperature plasma carbonitriding on cavitation erosion resistance of the Stellite 250 alloy – A preliminary evaluation, Wear 476 (2021), 203653, https://doi.org/10.1016/j.wear.2021.203653.
[6] A.K. Krella, Cavitation erosion of monolayer PVD coatings – An influence of deposition technique on the degradation process, Wear 478–479 (2021), 203762, https://doi.org/10.1016/j.wear.2021.203762.
[7] A. Bansal, J. Singh, H. Singh, D.K. Goyal, Influence of thickness of hydrophobic polytetrafluoroethylene (PTFE) coatings on cavitation erosion of hydro-machinery steel SS410, Wear 477 (2021), 203886, https://doi.org/10.1016/j.wear.2021.203886.
[8] T. Deplancke, O. Lame, J.-Y. Cavaille, M. Fivel, M. Riondet, J.-P. Franc, Outstanding cavitation erosion resistance of Ultra High Molecular Weight Polyethylene (UHMWPE) coatings, Wear 328–329 (2015) 301–308, https://doi.org/10.1016/j.wear.2015.01.077.
[9] C.E. Correa, G.L. García, A.N. García, W. Bejarano, A.A. Guzmán, A. Toro, Wear mechanisms of epoxy-based composite coatings submitted to cavitation, Wear 271 (2011) 2274–2279, https://doi.org/10.1016/j.wear.2011.01.088.
[10] D. Kowalski, M. Ueda, T. Ohtsuka, The effect of ultrasonic irradiation during electropolymerization of polypyrrole on corrosion prevention of the coated steel, Corros. Sci. 50 (2008) 286–291, https://doi.org/10.1016/j.corsci.2007.05.027.
[11] D.C. Gibson, J.R. Blake, The growth and collapse of bubbles near deformable surfaces, Appl. Sci. Res. 38 (1982) 215–224, https://doi.org/10.1007/BF00385951.
[12] J.R. Blake, D.C. Gibson, Cavitation bubbles near boundaries, Annu. Rev. Fluid Mech. 19 (1987) 99–123, https://doi.org/10.1146/annurev.fl.19.010187.000531.
[13] C.K. Turangan, B.C. Khoo, Transient bubble oscillations near an elastic membrane in water, J. Phys. Conf. Ser. 656 (2015) 12040, https://doi.org/10.1088/1742-6596/656/1/012040.
[14] A.H. Aghdam, B.C. Khoo, A note on the dynamics of two aligned bubbles perpendicular to and above a thin membrane, Fluid Dyn. Res. 47 (2015) 35503, https://doi.org/10.1088/0169-5983/47/3/035503.
[15] B.H.T. Goh, S.W. Gong, S.-W. Ohl, B.C. Khoo, Spark-generated bubble near an elastic sphere, Int. J. Multiph. Flow. 90 (2017) 156–166, https://doi.org/10.1016/j.ijmultiphaseflow.2016.03.021.
[16] S.J. Shaw, Y.H. Jin, T.P. Gentry, D.C. Emmony, Experimental observations of the interaction of a laser generated cavitation bubble with a flexible membrane, Phys. Fluids. 11 (1999) 2437–2439, https://doi.org/10.1063/1.870036.
[17] G.N. Sankin, P. Zhong, Interaction between shock wave and single inertial bubbles near an elastic boundary, Phys. Rev. E. 74 (2006) 46304, https://doi.org/10.1103/PhysRevE.74.046304.
[18] E.-A. Brujan, K. Nahen, P. Schmidt, A. Vogel, Dynamics of laser-induced cavitation bubbles near elastic boundaries: influence of the elastic modulus, J. Fluid Mech. 433 (2001) 283–314.
[19] A. Vogel, E.A. Brujan, P. Schmidt, K. Nahen, Interaction of laser-produced cavitation bubbles with an elastic tissue model, Proc.SPIE (2001), https://doi.org/10.1117/12.434701.
[20] A. Vogel, E.A. Brujan, P. Schmidt, K. Nahen, Interaction of laser-produced Cavitation bubbles with elastic boundaries, Fluid Mech. Its Appl. 62 (2001) 327–335, https://doi.org/10.1007/978-94-010-0796-2_40.
[21] S.W. Gong, S.W. Ohl, E. Klaseboer, B.C. Khoo, Scaling law for bubbles induced by different external sources: Theoretical and experimental study, Phys. Rev. E. 81 (2010) 56317, https://doi.org/10.1103/PhysRevE.81.056317.
[22] M. Dular, M. Petkovšek, On the mechanisms of cavitation erosion – Coupling high speed videos to damage patterns, Exp. Therm. Fluid Sci. 68 (2015) 359–370, https://doi.org/10.1016/j.expthermflusci.2015.06.001.
[23] S.H. Min, S. Wijesinghe, E.Y. Lau, M.L. Berkowitz, Damage to polystyrene polymer film by shock wave induced bubble collapse, J. Phys. Chem. B. 124 (2020) 7494–7499, https://doi.org/10.1021/acs.jpcb.0c04413.
[24] X. Qiao, R. Chen, H. Zhang, J. Liu, Q. Liu, J. Yu, P. Liu, J. Wang, Outstanding cavitation erosion resistance of hydrophobic polydimethylsiloxane-based polyurethane coatings, J. Appl. Polym. Sci. 136 (2019) 47668, https://doi.org/10.1002/app.47668.
[25] A. Krella, A. Czyzniewski, Influence of the substrate hardness on the cavitation erosion resistance of TiN coating, Wear 263 (2007) 395–401, https://doi.org/10.1016/j.wear.2007.02.003.
[26] A.K. Krella, D.E. Zakrzewska, M.H. Buszko, A. Marchewicz, Effect of thermal treatment and erosion aggressiveness on resistance of S235JR steel to cavitation and slurry, Materials (Basel). 14 (6) (2021) 1456.
[27] A.A. Voevodin, R. Bantle, A. Matthews, Dynamic impact wear of TiCxNy and Ti-DLC composite coatings, Wear 185 (1995) 151–157, https://doi.org/10.1016/0043-1648(95)06603-9.
[28] T.D. Raju, K. Nakasa, M. Kato, Relation between delamination of thin flims and backward deviation of load–displacement curves under repeating nanoindentation, Acta Mater. 51 (2003) 457–467, https://doi.org/10.1016/S1359-6454(02)00429-9.
[29] Z. Dong, T. Zhou, J. Liu, X. Zhang, B. Shen, W. Hu, L. Liu, Cavitation erosion behaviors of surface chromizing layer on 316L stainless steel, Ultrason. Sonochem. 58 (2019), 104668, https://doi.org/10.1016/j.ultsonch.2019.104668.
[30] R. Yang, X. Chen, Y. Tian, H. Chen, N. Boshkov, H. Li, An attempt to improve cavitation erosion resistance of UHMWPE coatings through enhancing thermal conductivity via the incorporation of copper frames, Surf. Coatings Technol. 425 (2021), 127705, https://doi.org/10.1016/j.surfcoat.2021.127705.
[31] Y. Sun, G. Xie, Y. Peng, W. Xia, J. Sha, Stability theories of nanobubbles at solid–liquid interface: A review, Colloids Surfaces A Physicochem. Eng. Asp. 495 (2016) 176–186, https://doi.org/10.1016/j.colsurfa.2016.01.050.
[32] V. Belova, D.A. Gorin, D.G. Shchukin, H. Möhwald, Controlled effect of ultrasonic cavitation on hydrophobic/hydrophilic surfaces, ACS Appl. Mater. Interfaces. 3 (2011) 417–425, https://doi.org/10.1021/am101006x.
[33] A. Kaffashi, A. Jannesari, Z. Ranjbar, Silicone fouling-release coatings: Effects of the molecular weight of poly(dimethylsiloxane) and tetraethyl orthosilicate on the magnitude of pseudobarnacle adhesion strength, Biofouling (Chur, Switzerland). 28 (2012) 729–741, https://doi.org/10.1080/08927014.2012.702342.
[34] W. Xu, Y. Zhai, J. Luo, Q. Zhang, J. Li, Experimental study of the influence of flexible boundaries with different elastic moduli on cavitation bubbles, Exp. Therm. Fluid Sci. 109 (2019), 109897, https://doi.org/10.1016/j.expthermflusci.2019.109897.
[35] N.S. Govinaa Rao, Cavitation- its inception and damage, Water Energy Int. 17 (1960) 516–543.